Electron Magnetic Reconnection Without Ion Coupling in Earth's Turbulent Magnetosheath

T. D. Phan[1], J. P. Eastwood[2], M. A. Shay[3], J. F. Drake[4], B. U. Ö. Sonnerup[5], M. Fujimoto[6], P. A. Cassak[7], M. Øieroset[1], J. L. Burch[8], R. B. Torbert[9], A. C. Rager[10,11], J. C. Dorelli[11], D. J. Gershman[11], C. Pollock[12], P. S. Pyakurel[3], C. C. Haggerty[3], Y. Khotyaintsev[13], B. Lavraud[14,], Y. Saito[6], M. Oka[1], R. E. Ergun[15], A. Retino[16], O. Le Contel[16], M. R. Argall[9], B. L. Giles[11], T. E. Moore[11], F. D. Wilder[15], R. J. Strangeway[17], C. T. Russell[17], P. A. Lindqvist[18], and W. Magnes[19]

[1]Space Sciences Laboratory, University of California, Berkeley, CA, USA

[2]The Blackett Laboratory, Imperial College London, London, UK

[3]University of Delaware, Newark, DE, USA

[4]University of Maryland, College Park, MD, USA

[5]Dartmouth College, Hanover, NH, USA

[6]ISAS/JAXA, Japan

[7]West Virginia University, Morgantown, WV, USA

[8]Southwest Research Institute, San Antonio TX, USA

[9]University of New Hampshire, Durham, NH, USA

[10]Catholic University of America, Washington DC, USA

[11]NASA Goddard Space Flight Center, Greenbelt, MD, USA

[12]Denali Scientific, Healy AK, USA

[13]Swedish Institute of Space Physics, Uppsala, Sweden

[14]Institut de Recherche en Astrophysique et Planétologie, Université de Toulouse, France

[15]University of Colorado LASP, Boulder, Colorado, USA

[16]CNRS/Ecole Polytechnique, Paris, France

[17]University of California, Los Angeles, Los Angeles, CA, USA

[18]Royal Institute of Technology, Stockholm, Sweden

[19]Space Research Institute, Austrian Academy of Sciences, Graz, Austria

Magnetic reconnection is a magnetic-to-particle energy conversion process fundamental to many space and laboratory plasma systems. In the standard model of reconnection, this process occurs in a minuscule electron-scale diffusion region around an X-line[1,2]. On larger scales, the ions couple to the newly-reconnected field lines and are ejected away from the X-line in the form of bi-directional ion jets at the ion Alfvén speed[3-5]. Much of the energy conversion occurs in spatially extended ion exhausts downstream of the diffusion region[6]. In turbulent plasmas, which contain a large number of small-scale current sheets, reconnection has long been suggested to play a major role in the dissipation of turbulent energy at kinetic scales[7-11]. However, experimental evidence for reconnection plasma jetting in small-scale turbulent plasmas has so far been lacking. Here we report the discovery in Earth's turbulent magnetosheath of an electron-scale current sheet where diverging bi-directional super-ion-Alfvénic electron jets, parallel electric fields, and enhanced magnetic-to-particle energy conversion were observed. Contrary to the standard reconnection picture, the thin reconnecting current sheet was not embedded in a wider ion-scale current layer and no ion jets were detected. Observations of this and other similar, but unidirectional, electron jet events without ion reconnection signatures reveal a new form of reconnection that can drive turbulent energy transfer and dissipation in electron-scale current sheets without ion coupling.

Turbulent magnetosheath regions downstream of Earth's quasi-parallel bow shock often contain hundreds of small-scale current sheets in which reconnection could potentially occur[9,10,12] (Figure 1c). Many are thin (ion inertial length scales or smaller), typically convecting past an observing spacecraft in a few seconds or less. If standard reconnection (Figure 1a) were to operate in turbulent current sheets, the ion jets in the extended exhausts should be the easiest reconnection signature to detect. Although electric field and magnetic field structures consistent with standard reconnection have been reported[9,10], in situ plasma measurements of the jets were not obtained for these thin current sheets because the data resolution using previous instruments (typically a few seconds per velocity measurement) was not sufficient to determine their presence or absence.

The four-spacecraft MMS mission, launched in 2015 and designed to reveal the kinetic physics of reconnection in near-Earth space, is flying in an electron-scale (~ 7-10 km) tetrahedral formation. It measures 3-D electron and ion distributions at up to 7.5 ms and 37.5 ms resolution[13], respectively, which are 400 times and 80 times better resolved than previously available data. MMS observations of turbulent magnetosheath current sheets have revealed thin current sheets[14], fast electron flows[15,16], and electron heating[12,16]. These characteristics are somewhat similar to those observed in the standard reconnection electron diffusion region in large-scale current sheets at the magnetopause[2,17] and in the laminar magnetosheath (that originate in the solar wind)[18,19]. However, ion jets, which should occur over a larger scale and therefore be more easily observed if standard reconnection is present in turbulent magnetosheath current sheets, remain elusive. This raises the question of whether fast electron flows in thin turbulent magnetosheath current sheets are produced by some process(es) besides reconnection.

Here we report the serendipitous simultaneous multi-spacecraft detection of oppositely directed super-ion-Alfvénic electron jets, parallel electric fields, and magnetic-to-particle energy conversion in an electron-scale current sheet in the magnetosheath, providing direct evidence for reconnection without ion-scale coupling in turbulence.

Figure 2a-c shows the large-scale context of the MMS observations in the subsolar magnetosheath region on December 9, 2016, 8:58-9:43 UT, with large fluctuations in both the magnetic field magnitude (Panel a) and its components (Panel b). Figures 2d-2g reveal these fluctuations to be sharp changes in the magnetic field associated with large current density spikes, many with $|\mathbf{j}| > 2\ \mu A/m^2$ and comparable to peak current densities observed in the electron diffusion region at Earth's magnetopause[2,17,20]. Such large current densities across magnetic field variations of a few tens of nT imply current sheet widths of a few tens of kilometers or less, i.e., below the ion inertial length (and ion gyroradius) of ~50 km in this interval. Closer inspection of the current density and magnetic field variations throughout the interval in Figures 2 reveals a range of current sheet thicknesses, i.e., many but not all are of sub-ion scales.

In order to distinguish the regular fast electron flows associated with any thin current sheet from electron jets due to reconnection, data should be examined in a current sheet (LMN) coordinate system. The current sheet normal points along **N**, **L** is along the anti-parallel magnetic field direction, and $\mathbf{M} = \mathbf{N}\times\mathbf{L}$ is in the out-of-plane (X-line) direction (Figure 1a). In such a frame, the main current is in the *M* direction, while the bi-directional reconnection outflows are in the $\pm L$ directions (Figure 1b). "Smoking gun" evidence for reconnection would be the simultaneous detection of oppositely directed plasma outflow jets by two spacecraft located on opposite sides of the X-line[4].

Such an event was captured at ~09:03:54 UT, when |**j**| reached ~ 3µA/m^2 (red arrow in Fig. 2g). Figure 3 shows in detail this current sheet, which had a magnetic shear of 14° (the guide field B_M ~ 40 nT, compared to anti-parallel field $|B_L|$ ~ 5 nT). Four spacecraft timing analysis finds the current sheet thickness to be only 4 km (or 4 electron skin depths, d_e), determined from the 45 ms crossing duration (between the vertical dashed lines in Figure 3) and the 95 km/s convection speed (V_N) of the current sheet.

Inside this electron-scale current sheet, both MMS 3 (left) and MMS 1 (right) observed fast out-of-plane electron flows V_{eM} ~ 900 km/s (Fig. 3c and 3m) that produced the main current j_M (Fig. 3d and 3n) and the associated B_L reversal (Fig. 3a and 3k). The V_{eM} speed is comparable to the inflow electron Alfvén speed, V_{AeL}, of 1000 km/s based on B_L ~ 5 nT and plasma density of 20 particles/cm^3.

Coincident with the intense current layers, MMS 3 and MMS 1 simultaneously observed oppositely directed electron jets in the outflow (L) direction, with ΔV_{eL}~ +250 km/s at MMS 3 (Fig. 3c) and ~ -450 km/s at MMS 1 (Fig. 3m), relative to an external V_{eL} flow of ~ +150 km/s. These electron outflow jets were ~10-18 times the asymptotic ion Alfvén speed (based on B_L), V_{AiL}, of ~25 km/s. As expected for a reconnection geometry with inflow from both sides, the changes in B_L for MMS 1 are correlated with those in V_{eL} in the first part of the field change and anti-correlated in the second half, while for MMS 3 the reverse holds. An exception to this behavior is that MMS 3, but not MMS 1, observed a ΔV_{eL} (~ -300 km/s) flow at the right-hand edge that is opposite to the main ΔV_{eL} flow (Fig. 3c). Simulations of standard reconnection with a strong guide field have shown such ΔV_{eL} edge flow[21]. The lack of an edge flow at MMS 1 is currently not understood.

The measurements of oppositely directed electron outflows at MMS 1 and MMS 3 are further supported by the higher resolution (0.125 ms) measurements of the L component of the field line velocity $\mathbf{E}\times\mathbf{B}/B^2$, which was negative at MMS 1 and positive at MMS 3 (except for a negative dip at the right edge, similar to V_{eL}) (Fig. 3q and 3g). The $(\mathbf{E}\times\mathbf{B}/B^2)_L$ outflows were predominantly perpendicular to the magnetic field due to the large B_M (Fig 3a and 3k); E_N (Fig. 3e and 3o), which is opposite at the 2 spacecraft, together with the dominant B_M, drives the outflows. Crucially, MMS 3 was located 7.1 km in the +L direction relative to MMS 1 so that the observations are consistent with diverging jets from a reconnection X-line located between the two spacecraft as they pass through the reconnecting current sheet. There was no evidence for ion jets (ΔV_{iL}) at the ion Alfvén speed (Fig. 3b,l) within the thin current sheet. That ion jets are absent is not surprising, because the current sheet thickness was only 0.09 d_i (or 0.09 ion gyroradii), and because the observations were made within 7 d_e of the X-line.

What is surprising, however, is that the electron-scale reconnecting current sheet was not embedded inside a much larger ion-scale current sheet as would be expected (and observed) in standard reconnection[1,18-20,22] (Fig. 1a). The absence of an outer ion-scale current sheet can be seen in Figures 3a and 3k (see also Extended Data Figure 1) which show B_L reaching its asymptotic values immediately outside the thin current sheet.

Both spacecraft detected well-defined parallel electric fields (Fig. 3f and 3p), implying that the electron frozen-in condition $\mathbf{E'} = \mathbf{E}+\mathbf{V}_e\times\mathbf{B} = 0$ was violated. Furthermore, $\mathbf{j}\bullet\mathbf{E'}$ was positive (Fig. 3j and 3t) and dominated by $j_{||}E_{||}$, indicating non-ideal magnetic-to-particle energy conversion[23] characteristic of the electron diffusion region. However, unlike standard reconnection where most of the magnetic energy is converted into ion jetting and heating, here, half of the (6 eV) available magnetic energy per particle in the inflow regions, $m_eV_{AeL}^2$, goes into kinetic energy associated with ΔV_{eM} and ΔV_{eL}, flowing at 90% and 45% of the electron Alfvén speed V_{AeL}, respectively. The remaining half (3 eV), if converted entirely into electron heating, would lead to a (3 eV) $(\gamma-1)/\gamma \approx 1$ eV electron temperature increase in the reconnecting current sheet[24], where $\gamma = 5/3$ is the ratio of specific heats. Such a small temperature increase would be not be discernable in the data (Fig. 3i and 3s).

Within the 21-minute burst data intervals shown in Figure 2a there were 34 other isolated current sheets with $|\mathbf{j}| > 2\ \mu A/m^2$ which implies sub-ion-scale current sheet widths. Surprisingly, the majority of these current sheets had low magnetic shears (i.e., strong guide fields): 23 of the 34 events had magnetic shear < 45°. All 34 showed fast out-of-plane electron velocity V_{eM} consistent with the large current density j_M, but only 16 displayed clear super-ion-Alfvénic V_{eL} jets that could be related to reconnection. In each of these cases, all four spacecraft detected V_{eL} pointing in the same direction and were therefore embedded in the same jet. The scarcity of unambiguous reconnection events with divergent jets and the X-line located between the spacecraft is likely due to the small (~ 7 km or 7 d_e) spacecraft separations.

We have found no evidence for reconnection ion jetting associated with any of the electron outflow jet events, or in any other (including ion-scale thick) current sheets in the 21-minute interval (see examples in Extended Data Figure 2). This finding is in stark contrast to standard models of reconnection where the ion exhaust jets should be easier to detect than the electron diffusion region because they extend large distances from the X-line.

The absence of ion reconnection signatures suggests that, in these turbulent magnetosheath plasmas, there is insufficient space and/or time for the ions to couple to the magnetic structures. This could occur not only because the current sheet widths are of electron scales, but also if the overall dimensions of the current sheets are limited because ion coupling requires some minimum lengths along the exhaust[25] (L) and X-line[26] (M) directions. A hybrid simulation study of resistive reconnection with no guide field[25] suggests that ions become decoupled when the length of the current sheet (in the L direction, e.g., Fig. 1c) falls below ~10 d_i. If such an electron-ion decoupling scale also exists in strong guide field collisionless reconnection, though potentially at a smaller scale than 10 d_i, it could account for our observed lack of ion coupling in magnetosheath reconnection, where the coherence scales of magnetic structures have been reported[27] to be of the order of d_i.

The experimental discovery of electron-only reconnection reveals that reconnection operates differently in current sheets with small overall dimensions. Our finding supports the long-held idea that reconnection plays a role in dissipating energy associated with plasma turbulence in space and astrophysical systems, although the scale for dissipation by reconnection would be at the electron scale instead of the ion scale. In order to quantitatively assess the importance of reconnection in dissipating turbulence energy in small systems, the basic properties of electron-only reconnection (e.g., the rate, duration, and onset conditions of reconnection) will need to be investigated both theoretically and observationally. They could differ significantly from our knowledge based on the standard reconnection paradigm.

References

1. Vasyliunas, V. M. Theoretical models of magnetic merging, *Rev. Geophys*, **13**, 1, 303-336, 1975.
2. Burch, J. L. *et al.* Electron-Scale Measurements of Magnetic Reconnection in Space, *Science,* **352**, 1189-1199 (2016).
3. Paschmann, G. *et al.* Plasma acceleration at the earth's magnetopause: Evidence for reconnection, *Nature* **282**, 243-246 (1979).
4. Phan, T. D. *et al.* Extended magnetic reconnection at the Earth's magnetopause from detection of bi-directional jets, *Nature*, **404**, 848-850 (2000).
5. Gosling, J. T. *et al.* Direct evidence for magnetic reconnection in the solar wind near 1AU, *J. Geophys. Res.*, **100**, A1 (2005).
6. Petschek, H. E., Magnetic field annihilation, in *AAS-NASA Symposium on the Physics of Solar Flares*, NASA Spec. Publ. SP-50, 425 (1964).
7. Matthaeus, W. H. and Lamkin, S. L. Turbulent magnetic reconnection, *Phys. Fluids*, **29**, 2513 (1986).
8. Servidio, S. *et al.* Magnetic reconnection in two-dimensional magnetohydrodynamic turbulence. Phys. Rev. Letters, **102** (2009).
9. Retinò, A. *et al. In situ* evidence of magnetic reconnection in turbulent plasma, *Nature Physics* **3**, 235 – 238 (2007).
10. Sundqvist, D. *et al.* Dissipation in Turbulent Plasma due to Reconnection in Thin Current Sheets, *Phys. Rev. Lett.* **99**, (2007).
11. Haggerty, C. C. *et al.* Exploring the statistics of magnetic reconnection X-points in kinetic particle-in-cell turbulence, *Physics of Plasmas*, **24**, 102308 (2017).
12. Chasapis, A. *et al.* Electron Heating at Kinetic Scales in Magnetosheath Turbulence, *Astro. Phys. J.*, **836**, 2, 247-255 (2017).
13. Rager, A. C. *et al.* Electron crescent distributions as a manifestation of diamagnetic drift in an electron scale current sheet: Magnetospheric Multiscale observations using new 7.5 ms Fast Plasma Investigation moments, *Geophys. Res. Lett.*, doi: 10.1002/2017GL076260 (2018).
14. Eriksson, E. *et al.* Strong current sheet at a magnetosheath jet: Kinetic structure and electron acceleration, *J. Geophys. Res.*, **121**, 10, 9608-9618 (2016).
15. Yordanova, E. *et al.* Electron scale structures and magnetic reconnection signatures in the turbulent magnetosheath, *Geophys. Res. Lett.*, **43**, 5969–5978 (2016).

16. Vörös, Z. *et al.* MMS observations of magnetic reconnection in the turbulent magnetosheath, *J. Geophys. Res.*, in press, (2017).
17. Chen, L. J. *et al.* Electron energization and mixing observed by MMS in the vicinity of an electron diffusion region during magnetopause reconnection, *Geophys. Res. Lett.*, **43**, 12, 6036-6043 (2016).
18. Phan, T. D. *et al.* Evidence for an elongated (> 60 ion skin depths) electron diffusion region during fast magnetic reconnection, *Phys. Rev. Lett.*, **99**, 25 (2007).
19. Wilder, F. D. *et al.* Multipoint measurements of the electron jet of symmetric magnetic reconnection with a moderate guide field, *Phys. Res. Lett.*, **118** (2017)
20. Burch, J. L. and Phan, T. D. Magnetic reconnection at the dayside magnetopause: Advances with MMS, *Geophys. Res. Lett.*, **43**, 16, 8327-8338 (2016).
21. Pritchett, P. L. Geospace Environment Modeling magnetic reconnection challenge: Simulations with a full particle electromagnetic code, *J. Geophys. Res.*, **106**, 3783-3798 (2001).
22. Shay, M. A. *et al.* Structure of the dissipation region during collisionless magnetic reconnection, *J. Geophys. Res.*, **103**, A5, 9165-9176 (1998).
23. Zenitani, S. *et al.* New Measure of the Dissipation Region in Collisionless Magnetic Reconnection, *Phys. Rev. Lett*. **106**, issue 19 (2011).
24. Shay, M. A. *et al.* Electron heating during magnetic reconnection: A simulation scaling study, *Phys. Plasmas,* **21**, 122902:1-11 (2014).
25. Mandt, M. E. *et al.* Transition to whistler mediated magnetic reconnection, *Geophys. Res. Lett.*, **21**, 1, 73-76 (1994).
26. Meyer, J. C. Structure of the diffusion region in three dimensional magnetic reconnection, PhD thesis, University of Delaware (2015).
27. He, J. S. *et al.* Two-dimensional correlation functions for density and magnetic field fluctuations in magnetosheath turbulence measured by the Cluster spacecraft, J. *Geophys. Res.*, **116**, A6, CiteID A06207 (2011).
28. Torbert, R. B. *et al.* The FIELDS Instrument Suite on MMS: Scientific Objectives, Measurements, and Data Products, Space Sci. Rev., (2014).
29. Gosling, J. T. and Phan T. D. Magnetic reconnection in the solar wind at current sheets associated with extremely small field shear angles, *Astrophys. J. L.*, **763** (2013).
30. Sonnerup, B. U. Ö., Cahill Jr., L. J. Magnetopause structure and attitude from Explorer 12 observations, *J. Geophys. Res.*, **96**, 72, 171 (1967).

Acknowledgments. We are grateful for the dedicated efforts of the MMS team. This work was supported by NASA Contract No. NNG04EB99C at SwRI, which funded work at most of the co-author institutions in the United States. The work at U.C. Berkeley was supported by NASA grant NNX08AO83G. UK involvement at Imperial College was supported by STFC (UK) grant ST/N000692/1. The French involvement (SCM instruments) on MMS is supported by CNES, CNRS-INSIS and CNRS-INSU.

Author Contributions T. D. P. carried out the data analysis, interpretation, and manuscript preparation. J.P.E, M.A.S, J.F.D, B.U.Ö.S., M.F., P.A.C., M.Ø., P.S.P., C.H., M.O, and A.R. contributed to the data interpretation and manuscript preparation. J. L. B led the successful design and operation of the MMS mission and contributed to the interpretation of the data. A.C.R., J.C.D., D.J.G., C. P., B.L, B.L.G, T.E.M, and Y.S. contributed to the development, operation, and interpretation of data from the Fast Plasma Instruments. R.B.T., R.E.E., Y.K., M.R.A., F.D.W. and P.A.L. contributed to the development, operation, and interpretation of data from the electric field experiments. O.L.C. contributed to the development and operation of the search-coil magnetometers. C.T.R., R.J.S, and W.M. contributed to the development and operation of the fluxgate magnetometers.

Author Information. Reprints and permissions information is available at www.nature.com/reprints. The authors declare no competing financial interests. Correspondence and requests for materials should be addressed to T.D.P (phan@ssl.berkeley.edu).

Data availability. The entire MMS data set is publicly available on-line at https://lasp.colorado.edu/mms/sdc/public/.

Main Figure Legends

Figure 1. Schematics contrasting (a) standard magnetic reconnection in large-scale current sheets and (b, c) electron-only reconnection in small-scale turbulence. The reconnection configurations in panels (a) and (b) are displayed in the current sheet (LMN) coordinate system. (a) In standard reconnection, the magnetic topology changes in the small electron diffusion region (EDR) around the X-line, but most of the magnetic-to-particle energy conversion happens in the extended exhausts, with bidirectional ion jetting and heating. The EDR width (along **N**) is of the order of an electron skin depth (d_e), while its length along $\pm L$ could be up to a fraction of an ion inertial length $d_i = 43\ d_e$. The EDR is embedded in an ion diffusion region (IDR), while the magnetohydrodynamic-scale reconnection exhaust can extend thousands of d_i (along **L**) away from the X-line[5]. (b) Schematics of reconnection in an electron-scale current sheet involving only electrons, with no ion coupling. The entire current sheet is essentially the electron diffusion region having a single (electron) scale with embedded bi-directional super-ion-Alfvénic jets. Overlaid are MMS 1 and 3 trajectories through the current sheet relative to the X-line deduced based on the electron jet directions observed on 2016-12-09 at ~09:03:54 UT (and shown in Figure 3). MMS 1 and 3 were on opposite sides of the X-line detecting bi-directional electron jets. The slanted spacecraft trajectories take into account the likely motion (in the spacecraft frame) of the X-line due to the presence of an external electron flow along $+L$ of ~150 km/s. (c) Schematic showing the formation of multiple small (d_i)-scale magnetic structures and thin (d_e-scale) current sheets at their interfaces in turbulent plasmas, informed by turbulence simulations[8,12].

Figure 2. Overview of MMS 1 observations of turbulent current sheets in Earth's subsolar magnetosheath region downstream of a quasi-parallel shock, showing the presence of large current density spikes (>2 μA/m^2) implying sub-ion-scale current sheets. The data is displayed in the geocentric solar ecliptic (GSE) coordinates. (a, b) The magnetic field magnitude and components. (c) The ion energy-time spectrogram of differential energy flux (eV s^{-1} cm^{-2} ster^{-1} eV^{-1}). (d-g) Zoomed-in (4-minute) interval showing the magnetic field, ion velocity, electron velocity, and current density computed from plasma measurements $\mathbf{j} = eN_e(\mathbf{V_i}-\mathbf{V_e})$. Throughout the interval in panels a-c, the angle between the interplanetary magnetic field and X_{GSE} was less than 30° and the subsolar bow shock was quasi-parallel. The current density spike

at ~09:03:54 UT (indicated by the red arrow in panel g) is the bi-directional electron jet event to be shown in detail in Figure 3. Red horizontal bars in panel a denote burst data intervals totaling 21 minutes selected by the MMS scientist-on-duty because they contained a large number of high amplitude magnetic field fluctuations (with Δ**B**/*B* ~ 0.5) suggestive of current sheets that could be prone to reconnection.

Figure 3. MMS 1 and 3 simultaneous detections of oppositely directed super-ion-Alfvénic electron jets, parallel electric fields, and enhanced magnetic-to-electron energy conversion in an electron-scale current sheet. The data for both spacecraft are shown in a common current sheet (LMN) coordinate system determined for the MMS 3 crossing of the current sheet at 09:03:54.270 – 09:03:54.365 UT, with $\mathbf{L}$= $(-0.091, 0.87, 0.49)_{GSE}$, $\mathbf{M}$= $(-0.25, -0.49, 0.83)_{GSE}$, and $\mathbf{N}$= $(0.96, -0.05, 0.27)_{GSE}$. (a,k) Magnetic field at 8196 samples/s (from merged fluxgate and search-coil magnetometer measurements[28]), with B_M shifted by -30 nT. (b,c and l,m) Ion and electron velocity. The 7.5 ms electron and 37.5 ms ion data products were generated by separating the individual energy sweeps used to form the nominal burst-mode distribution functions. These data maintain sufficient angular coverage to recover accurate plasma moments at 4 times the nominal temporal resolution[13]. (d,n) Current density from plasma measurements. (e,o) Electric field[28] in the spacecraft frame at 8196 samples/s. (f,p) Electric field component parallel to the magnetic field. (g,q) $\mathbf{E}\times\mathbf{B}/B^2$ velocity. (h) Electron density. (i) Electron temperature. (j,t) $\mathbf{j}\bullet(\mathbf{E}+\mathbf{V}_e\times\mathbf{B})$. The LMN coordinate system was determined using a hybrid minimum variance method which often works best in low magnetic shear current sheets[29]. The current sheet normal direction, $\mathbf{N}$, was determined from $\mathbf{B_1}\times \mathbf{B_2} /| \mathbf{B_1}\times \mathbf{B_2}|$, where $\mathbf{B_1}$ and $\mathbf{B_2}$ are the fields at the two edges of the current sheet. $\mathbf{M} = \mathbf{L'}\times\mathbf{N}$, where $\mathbf{L'}$ is the maximum variance direction from the minimum variance of the magnetic field[30]. $\mathbf{L}= \mathbf{N}\times\mathbf{M}$. MMS 3 was located at *L*= +7.1 km, *M*= +3.3 km, and *N*= +1.6 km relative to MMS1. Data from all 4 spacecraft are shown in Extended Data Figure 3.

Extended Data Figure Legends

Extended Data Figure 1. Large-scale context of the thin current sheet shown in Figure 3, illustrating the fact that the electron-scale current sheet was a stand-alone current sheet not embedded inside an ion-scale current sheet. Data is shown in LMN coordinates determined for the thin current sheet and used in Figure 3. (a) Magnetic field. (b) Ion velocity. (c) Electron velocity. (d) $\mathbf{j}\bullet(\mathbf{E}+\mathbf{V}_e\times\mathbf{B})$. The thin reconnecting current sheet stands out in this interval, with nothing else approaching its current density or its value of $\mathbf{j}\bullet(\mathbf{E}+\mathbf{V}_e\times\mathbf{B})$. The absence of an ion-scale current sheet enveloping the electron-scale current sheet is indicated by the fact that $|B_L|$ reaches essentially its asymptotic values immediately outside the thin current sheet.

Extended Data Figure 2. Absence of reconnection ion jetting. The data is in GSE coordinates. (a) Magnetic field. (b) Ion velocity. (c) *Y* component of the ion velocity, V_{iy}, and Alfvén velocity, V_{Ay}. (d) *Z* component of the ion velocity, V_{iz}, and Alfvén velocity, V_{Az}. $\mathbf{V_A}$ is relative to the reference velocity, density, and magnetic field values at the left edge of the data interval: $\mathbf{V}_A = \mathbf{B}_{\mathrm{ref}}(1-\alpha_{ref})^{1/2}(\mu_0\rho_{ref})^{-1/2} - \mathbf{B}(1-\alpha)^{1/2}(\mu_0\rho)^{-1/2}$, where $\alpha = (p_{//}-p_\perp)\mu_0/B^2$ is the pressure anisotropy factor and ρ is the plasma mass density[3]. The expected speeds of the ion reconnection jets embedded inside many of the large magnetic shear current sheets are in the range of 100-200 km/s, based on B_L variations of the order of 20-40 nT (panel a). If present, such jets are readily recognized by back-to-back opposite correlations between ion velocity and magnetic field variation at the two edges of the current sheet as indications of pairs of rotational discontinuities emanating from the X-line[5]. These signatures are not seen here. What one finds instead in the data is either no correlation between components of $\mathbf{V_i}$ and $\mathbf{B}$, or single correlation (or anti-correlation), indicative of Alfvénic structures[16] rather than reconnection jetting.

Extended Data Figure 3. Four-spacecraft observations of the reconnecting current sheet shown in Figure 3. A common current sheet LMN coordinate system (same as in Figure 3) was used for consistency, and supported by the fact that the LMN coordinates at individual spacecraft differ from each other by less than 4°. (a,b) *L* and *M* components of the magnetic field, (c,d) *L* and *M* components of the electron velocity. (e) *M* component of the current density. (f) *L* component of the $\mathbf{E}\times\mathbf{B}/B^2$ velocity, (g) N component of the electric field. (h) electric field component parallel to the magnetic field, (i) $\mathbf{j}\bullet(\mathbf{E}+\mathbf{V}_e\times\mathbf{B})$, and (j) spacecraft locations relative to MMS 1, in km (~d_e). The B_L profiles (panel a) show that MMS 1 and 3 crossed the current sheet at essentially the same time, preceded by MMS 4 and followed by MMS 2. The fact that MMS 4 exited the current sheet before MMS 2 entered it places an upper limit on the current sheet thickness, which is the 4.5 km separation distance between the 2 spacecraft along **N** (panel f). This is consistent with the 4 km current sheet width determined from the motion and crossing duration of the current sheet. Inside the current sheet, MMS 4 detected a positive $(\mathbf{E}\times\mathbf{B}/B^2)_L$ (except at the right edge) similar to MMS 3, whereas MMS 2 detected a negative $(\mathbf{E}\times\mathbf{B}/B^2)_L$ similar to MMS 1. This indicates that there was a pair of spacecraft on each side of the X-line. All 4 spacecraft detected a predominantly negative $E_{||}$. The parameter $\mathbf{j}\bullet(\mathbf{E}+\mathbf{V}_e\times\mathbf{B})$ was consistently positive at all 4 spacecraft throughout the current sheet, with the amplitude being lowest at MMS 2. MMS 2 also detected the largest guide field (B_M) compression, fastest ΔV_{eL} and $(\mathbf{E}\times\mathbf{B}/B^2)_L$ flows, slowest ΔV_{eM} and weakest $E_{||}$, which together may suggest that MMS 2 was furthest away from the X-line.

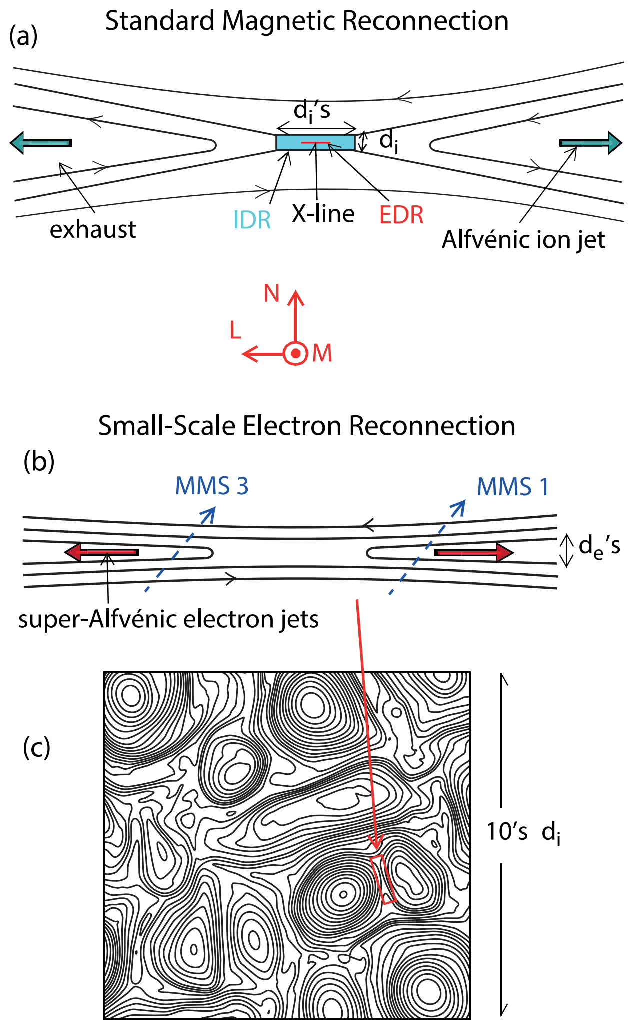

(a)
Standard Magnetic Reconnection
d_i's
d_i
exhaust
IDR
X-line
EDR
Alfvénic ion jet
N
L
M
Small-Scale Electron Reconnection
(b)
MMS 3
MMS 1
d_e's
super-Alfvénic electron jets
(c)
10's d_i

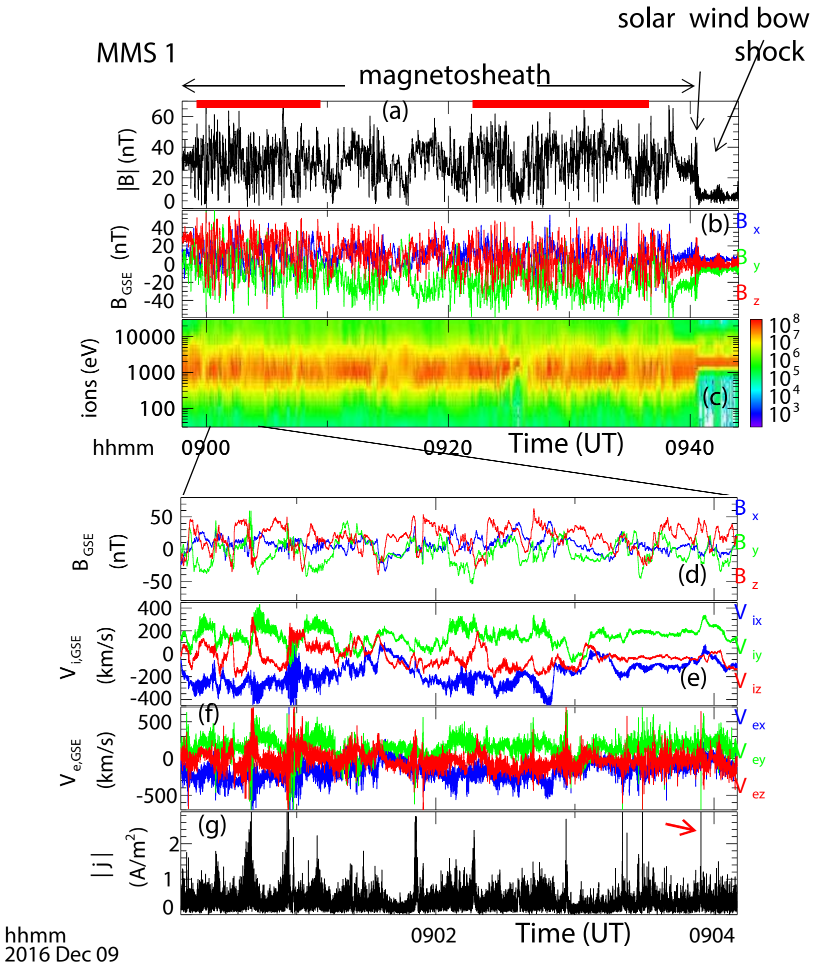
MMS 1
magnetosheath
solar wind
bow shock
(a)
|B| (nT)
(b)
B_GSE (nT)
B x
B y
B z
ions (eV)
(c)
hhmm
0900
0920
0940
Time (UT)
(d)
(e)
V_i,GSE (km/s)
V ix
V iy
V iz
(f)
V_e,GSE (km/s)
V ex
V ey
V ez
(g)
|j| (A/m²)
0902
0904
hhmm
2016 Dec 09

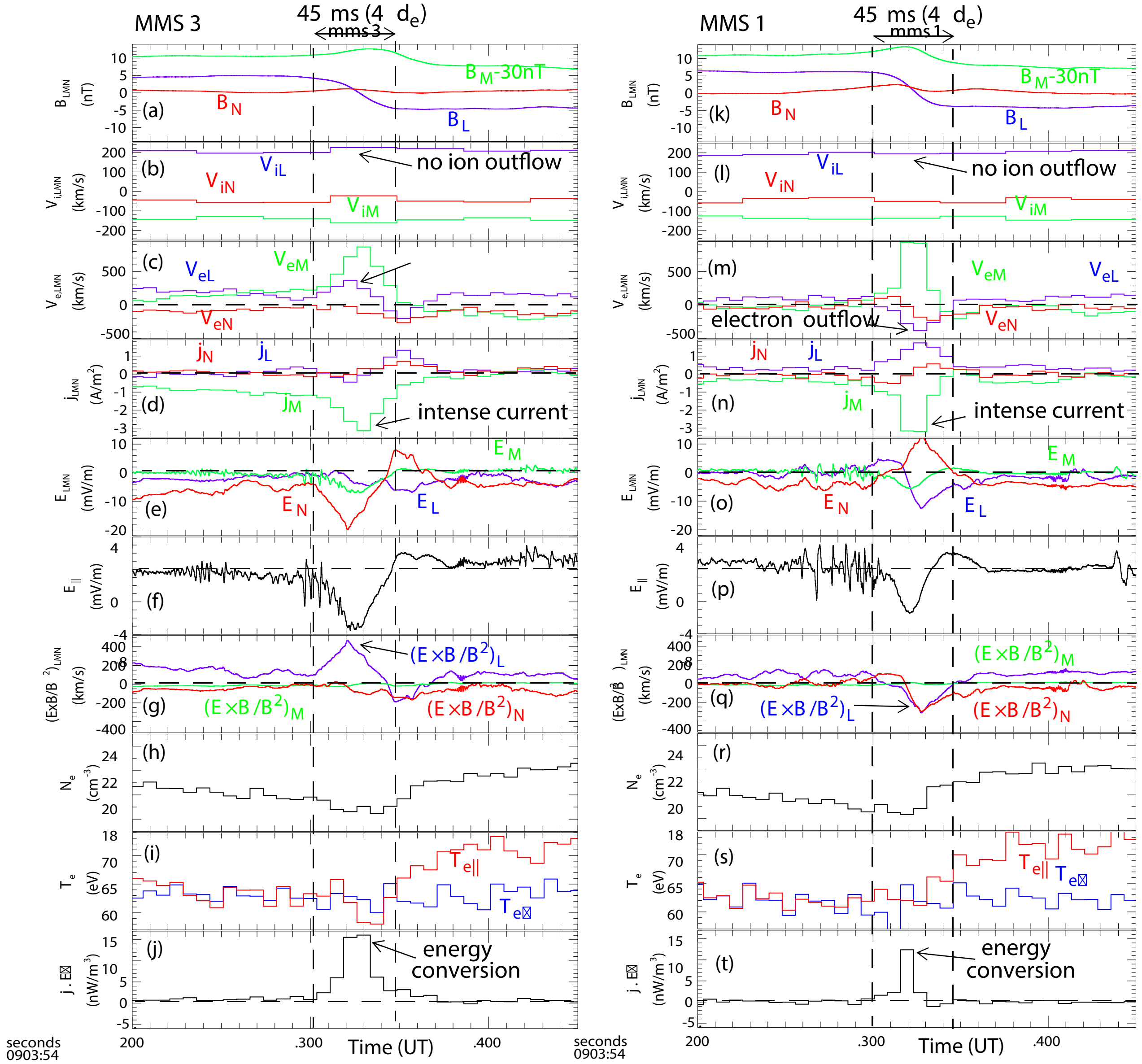

MMS 3
45 ms (4 de)
mms 3
MMS 1
45 ms (4 de)
mms 1
BM-30nT
BN
BL
no ion outflow
ViL
ViN
ViM
VeL
VeM
VeN
electron outflow
jN
jL
jM
intense current
EM
EN
EL
(E×B/B2)L
(E×B/B2)M
(E×B/B2)N
Te∥
energy conversion
Time (UT)
seconds 0903:54

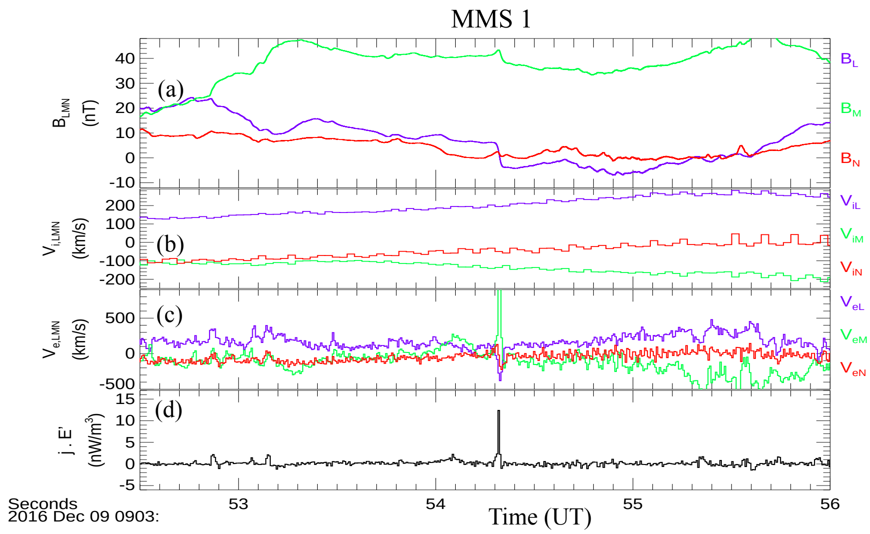

MMS 1
(a)
B_{LMN} (nT)
40
30
20
10
0
-10
B_L
B_M
B_N
(b)
$V_{i,LMN}$ (km/s)
200
100
0
-100
-200
V_{iL}
V_{iM}
V_{iN}
(c)
$V_{e,LMN}$ (km/s)
500
0
-500
V_{eL}
V_{eM}
V_{eN}
(d)
j . E' (nW/m^3)
15
10
5
0
-5
Seconds
2016 Dec 09 0903:
53
54
55
56
Time (UT)

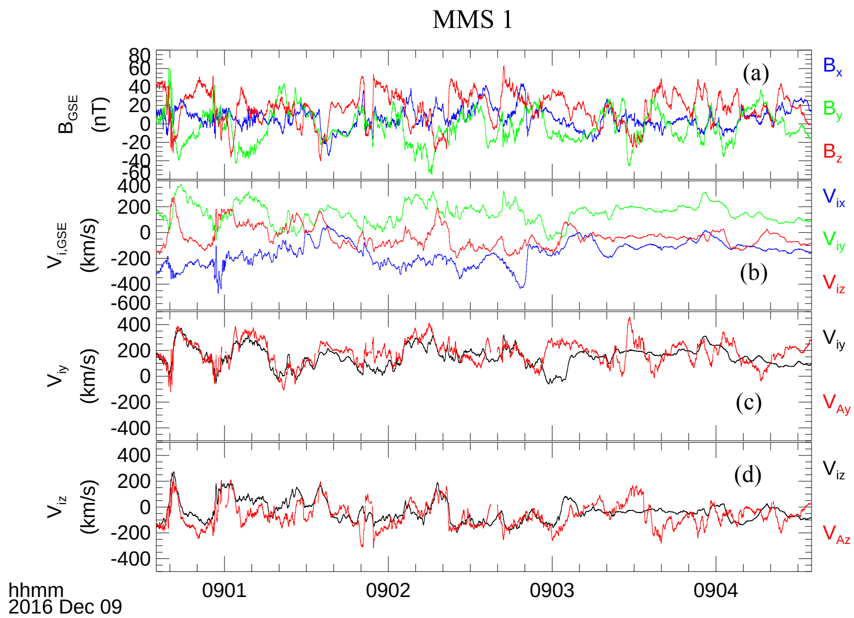

MMS 1
(a)
(b)
(c)
(d)
B_GSE (nT)
V_i,GSE (km/s)
V_iy (km/s)
V_iz (km/s)
Bx
By
Bz
Vix
Viy
Viz
Viy
VAy
Viz
VAz
hhmm
2016 Dec 09
0901
0902
0903
0904

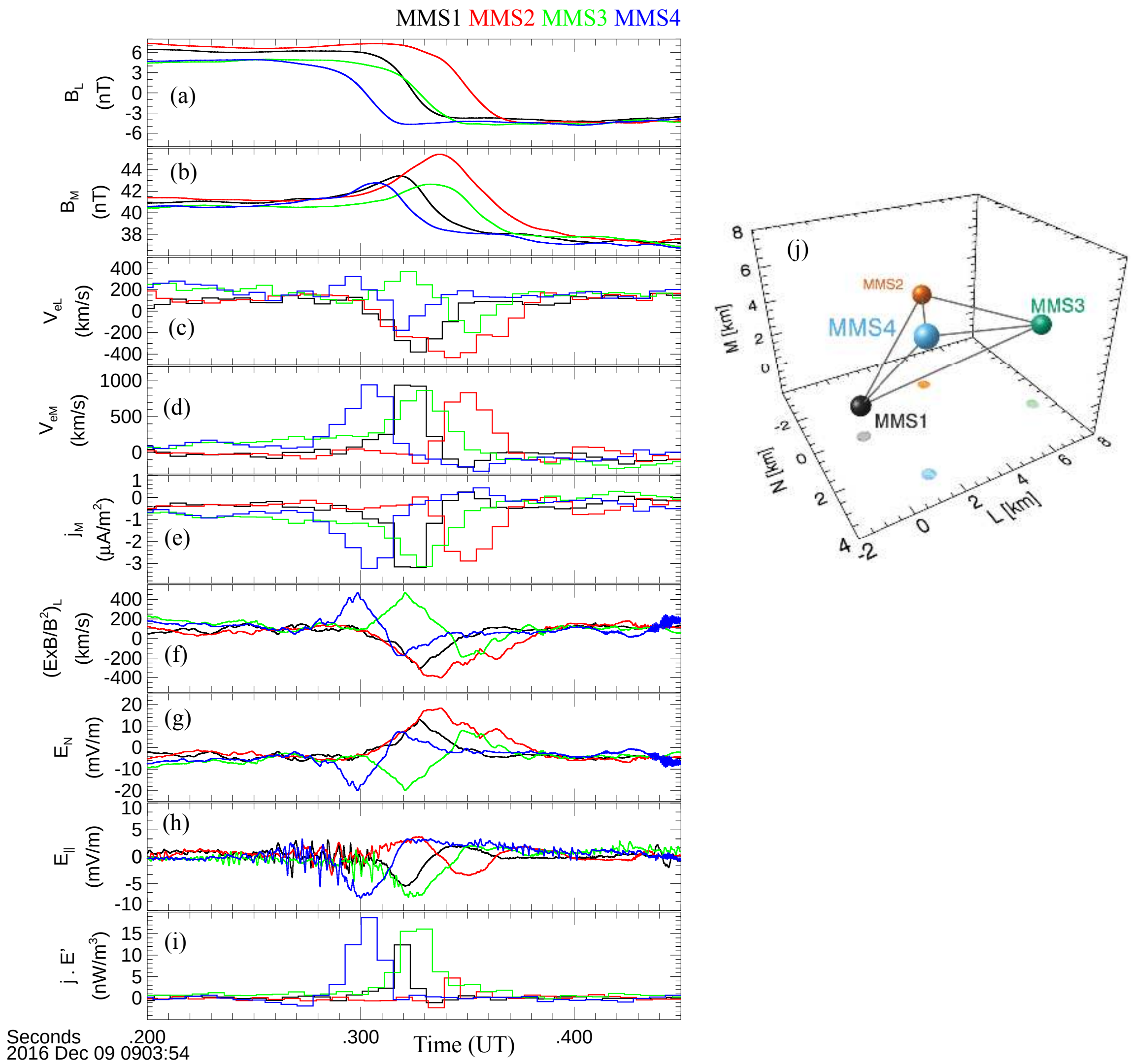
MMS1 MMS2 MMS3 MMS4
(a)
(b)
(c)
(d)
(e)
(f)
(g)
(h)
(i)
(j)
Seconds .200 .300 .400
2016 Dec 09 0903:54
Time (UT)
MMS2
MMS3
MMS4
MMS1
M [km]
N [km]
L [km]